第 15 回日本地震工学シンポジウム（2018）

EXPERIMENTAL INVESTIGATION ON ULTIMATE DRIFT CAPACITY OF RC BEAMS SUBJECTED TO REVERSE CYCLIC LOADING: PHOTOGRAMMETRIC OBSERVATIONS

Shubham TRIVEDI[1], Hitoshi SHIOHARA[2], and Seitaro TAJIRI[3]

1) Ph.D. Candidate, Department of Architecture, The University of Tokyo,
shubham@rcs.arch.t.u-tokyo.ac.jp
2) Professor, Department of Architecture, The University of Tokyo,
shiohara@arch.t.u-tokyo.ac.jp
3) Associate Professor, Department of Architecture, The University of Tokyo,
tajiri@arch.t.u-tokyo.ac.jp

ABSTRACT: An innovative measurement scheme using digital camera and photogrammetric analysis was employed to study detailed beam specimen response. Instrumentation and analysis algorithm utilized are explained. Lateral, axial and shear strains deduced from the recorded surface deformations are discussed. Photogrammetric observations help better understanding of beam response by allowing comprehensive and detailed comparison of strain quantities not measurable with conventional instruments. Accumulation of lateral and shear strain in the beam hinge zone is identified to be closely related to the loss of load resisting capacity in beams at large deformation cycles.

Keywords: Photogrammetry, Beam experiment, Cyclic loading, Ultimate deformation

1. INTRODUCTION

Strong focus on the development of strength-based design of buildings in the past has led to significant improvements in determination of element strengths. Estimation of deformation, however, has remained a more difficult task. Although this design requires a minimum amount of ductility in elements to develop the required strength, accurate estimates of the deformation capacity are not explicitly required. With the advent of performance-based design, accurate assessment of deformation capacity has become increasingly important. Success of performance-based design in achieving efficiency and economy is dependent on the accuracy and reliability of the deformation capacity estimation.

In a recently concluded experimental investigation by Trivedi [1)], sixteen RC beams were tested to study deformation response at limit state. Parameters considered included: concrete strength, transverse reinforcement content, shear-span, transverse reinforcement strength and longitudinal reinforcement content. While a general understanding of the influence of the individual parameters was established, no concluding observations could be made on the underlying mechanism for determining the deformation capacity. In this report, photographic data recorded during the experiment is analyzed and discussed to possibly reveal more conclusive evidence on the mechanism determining the deformation capacity.

2. PHOTOGRAMMETRIC MEASUREMENTS

2.1. Instrumentation

Basic instrumentation for realizing photogrammetric measurements was designed to accommodate two primary requirements: a digital camera to continuously shoot at and record the state of concrete specimen surface, and an appropriately prepared specimen surface affixed with targets of a special pattern. Canon EOS 750D, a digital single-lens reflex camera with Canon EF-S18-55mm lens was used to record the images during the experiment. The camera was fixed to a stiff reference frame to ensure a common reference for all images. The reference frame was in turn attached to the specimen stub as shown in Figure 1. The photographed surface was affixed with targets on a 50 mm-by-50 mm grid covering 200 mm of 240 mm of the section width and 500 mm of 700 mm of the loading span of the beam as illustrated in Figure 2. Concrete surface was lightly painted in white to provide a good contrast to the black target pattern. Each target consisted of a special pattern printed on a thick (0.335 mm) white paper and cut in small sized (20 mm) squares. These targets were fixed on the surface using small strips (5 mm-by-5 mm) of a thick two-sided tape. This arrangement ensured that the targets had a small but strong contact with specimen surface and made it less likely for the target to fall in the path of surface cracks and thus remain in place for longer.

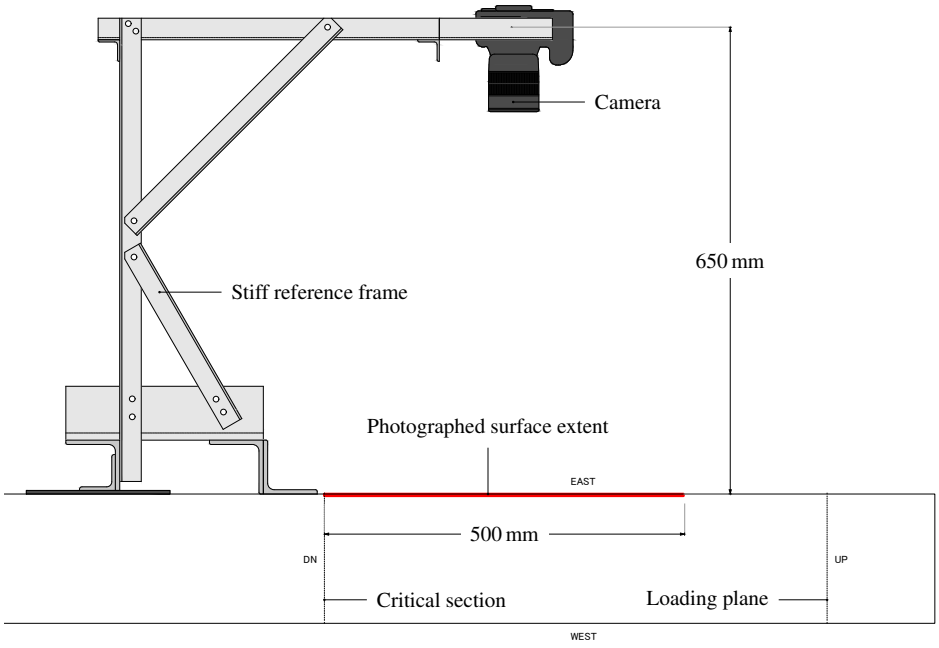

Figure 1: Reference frame and camera arrangement for recording images

Using this arrangement a continuous stream of images were recorded throughout the loading duration. The timestamp of each recorded image was corresponded with the loading data to determine the position of each image on the loading time-history.

2.2. Photogrammetric analysis

Concrete surface deformation was tracked by monitoring the position of each target in each recorded image. Target locations in each image were digitally determined using the image-processing concept of pattern-matching. This essentially involves calculating a correlation function to compare the original and displaced images. Displaced image position can be identified as the location of the peak of the correlation

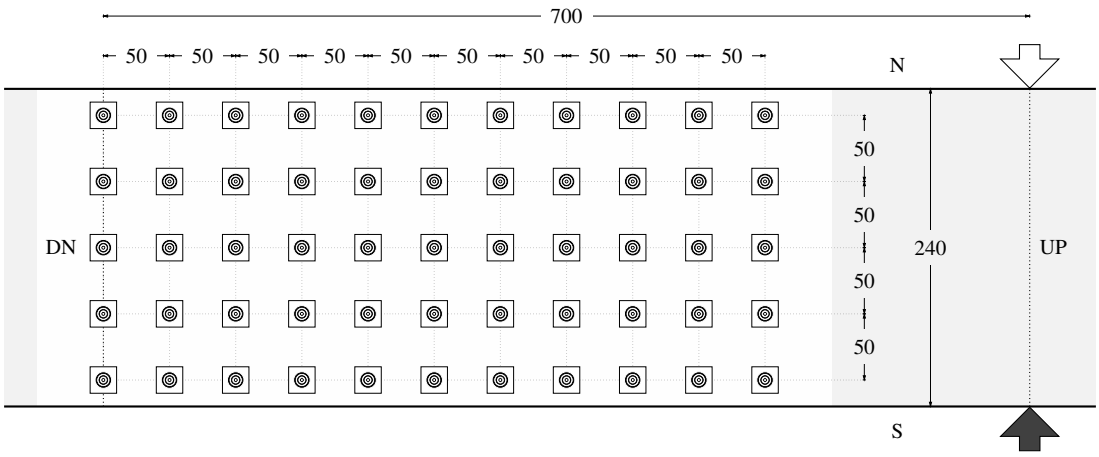

Figure 2: Photogrammetric grid (all dimensions in mm)

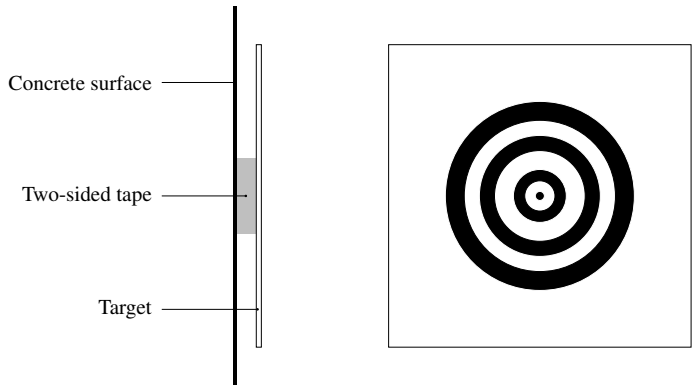

Figure 3: Target affixation to concrete surface

function[2]. In this study, normalized fourier cross-correlation was used as the correlation function to identify the location of targets in the image.

Target locations identified from the image in pixel coordinates are transformed to distance coordinates using intrinsic parameters of the camera. In this study, camera parameters are measured by using chequered patterns based on the approach suggested by Zhang[3]. A chequered pattern of known square sizes was printed and shot at various angles and distances from the camera. Corner locations of squares in the recorded images were identified and compared with know pattern dimensions to determine the camera intrinsic parameters.

2.3. Strain calculation

Once the identified target locations in each image frame are resolved in appropriate coordinates, specimen behavior can be studied by calculating various surface strain quantities. In this research, beam response is studied in terms of three strain quantities: lateral strain across the beam width, axial strain along the beam span, and shear strain on the surface.

Grid space on the concrete surface is defined using a set of horizontal (Y_j) and vertical (X_i) grids as expressed in Figure 4. At any recorded frame n, the coordinates x^n_{ij} and y^n_{ij} of any point X_iY_j on this grid plane are defined in reference to the origin O located at critical section of the specimen. Distance between any two points X_aY_b and X_cY_d is determined at the respective frame n as:

$$l^n_{abcd} = \sqrt{(x^n_{ab} - x^n_{cd})^2 + (y^n_{ab} - y^n_{cd})^2} \tag{1}$$

Lateral strain is calculated at each vertical grid $X_i(i = 1:10)$ by measuring the respective deformations across the two extreme horizontal grids Y_1 and Y_5 as:

$$\varepsilon^n_{lateral_i} = \frac{l^n_{i1i5} - l^1_{i1i5}}{l^1_{i1i5}} \tag{2}$$

Axial strain is calculated at each vertical grid $X_i(i = 1:10)$ by measuring the average deformation across all horizontal grids $Y_j(j = 1:5)$ as:

$$\varepsilon^n_{axial_i} = \frac{\sum_{j=1}^{5} l^n_{ij1j} - \sum_{j=1}^{5} l^1_{ij1j}}{\sum_{j=1}^{5} l^1_{ij1j}} \tag{3}$$

Shear strain is calculated using the concept of principle strains for basic triangular elements as shown in Figure 5. Entire grid is divided into small triangular elements and principal strain components for each element at any frame n are given as:

$$\varepsilon^n_x = \frac{(x^n_{i+1j} - x^n_{ij}) - (x^1_{i+1j} - x^1_{ij})}{(x^1_{i+1j} - x^1_{ij})} \tag{4}$$

$$\varepsilon^n_y = \frac{(y^n_{ij-1} - y^n_{ij}) - (y^1_{ij-1} - y^1_{ij})}{(y^1_{ij-1} - y^1_{ij})} \tag{5}$$

$$\varepsilon^n_{xy} = \frac{(x^n_{ij-1} - x^n_{ij}) - (x^1_{ij-1} - x^1_{ij})}{(y^1_{ij-1} - y^1_{ij})} + \frac{(y^n_{i+1j} - y^n_{ij}) - (y^1_{i+1j} - y^1_{ij})}{(x^1_{i+1j} - x^1_{ij})} \tag{6}$$

Note that all strains are expressed with respect to the initial undeformed state at frame 1.

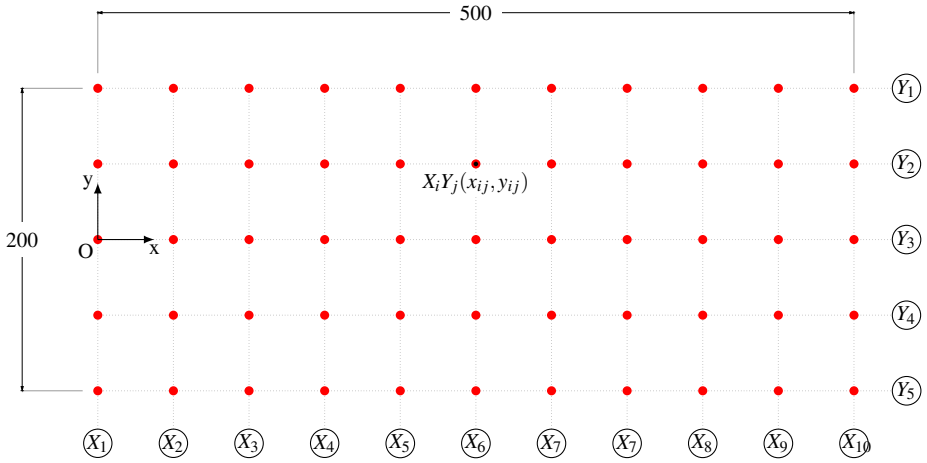

Figure 4: Strain measurement grid (all dimensions in mm)

3. ANALYSIS RESULTS

A sample of the recorded deformation trace of the targets at each observation grid for one of the specimens (SB05) over the entire loading history is expressed in Figure 6. This static image offers a quick

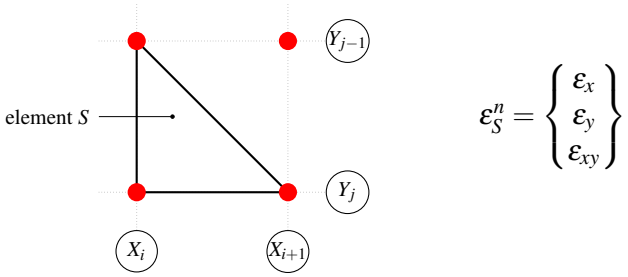

Figure 5: Fundamental element for principal strain calculation.

visualization of beam response under cyclic loading. All 55 targets do not trace perfect radial paths as would be the case for purely flexural response but most targets near the hinge traverse a smaller range of displacements than the targets close to the tip. These target displacements are individually analyzed to study lateral, axial and shear strain development in the specimens.

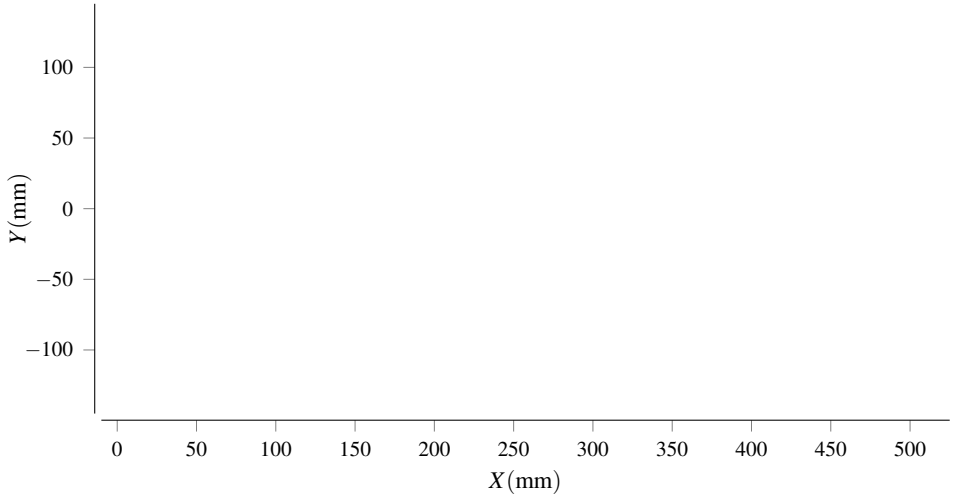

Figure 6: An example of deformation trace calculated with photogrammetric analysis (for specimen SB05)

Lateral strain over the vertical grid locations as defined by Equation (2) is expressed for all specimens in Figure 7. These curves show the extent and development of bulging in the hinge region. Each curve represents the state of specimen at zero total drift after being exposed to multiple cycles of load application in both positive and negative directions. The solid line represents the state at completion of three cycles while the lighter lines represent the state after one or two cycles of loading. The respective target drift levels are indicated by the thickness of the curves. States for target drift levels 2 %, 3 % and 4 % are illustrated for all specimens. Note that some absurdly high or negative strain values are frequently observed in the figures. This is due to dislocation of the targets which becomes increasingly common with extensive cracking on the concrete surface at larger drifts.

Comparing specimens SB-01 and SB-04 we can immediately see the effect of closely spaced stirrups. Very limited strains are observed in SB-04 and most bulging is restricted to a small region close to the critical section. Bulging in SB-01 is both excessive and extensive in comparison. This observation is generally true for respective comparisons between the series of specimens in the first and second rows. SC series specimens had transverse reinforcement content exceeding 1 % and therefore exhibit very limited development of lateral strains.

Axial strains at respective vertical grid location as defined by Equation (3) are similarly expressed for all specimens in Figure 8. One striking difference from the lateral strain development is the negligible

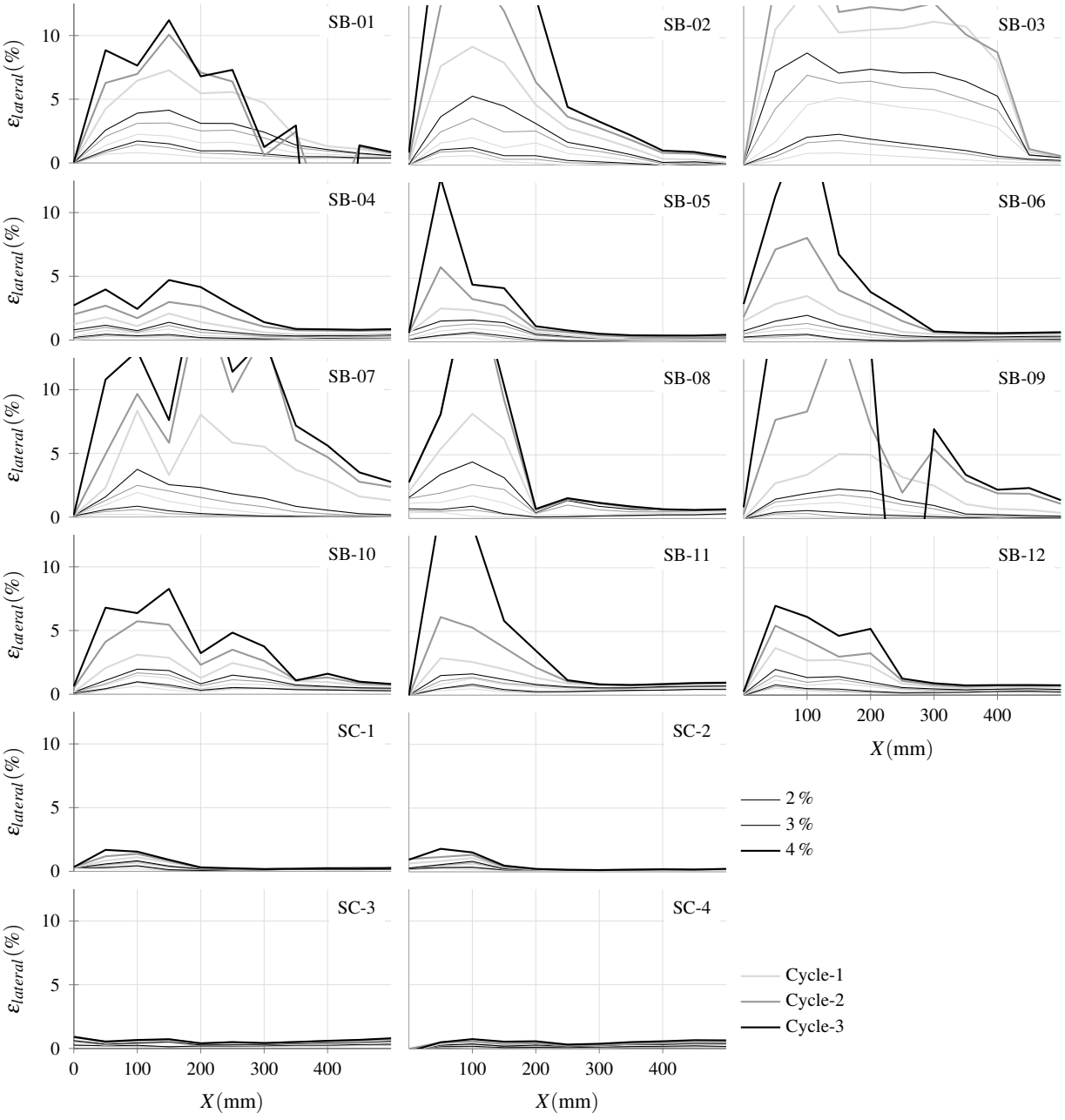

Figure 7: Lateral strain profiles for all specimens at the end of 3 (thick lines), 2, and 1 (thin lines) loading cycles at increasing target drifts (2 %, 3 % and 4 %)

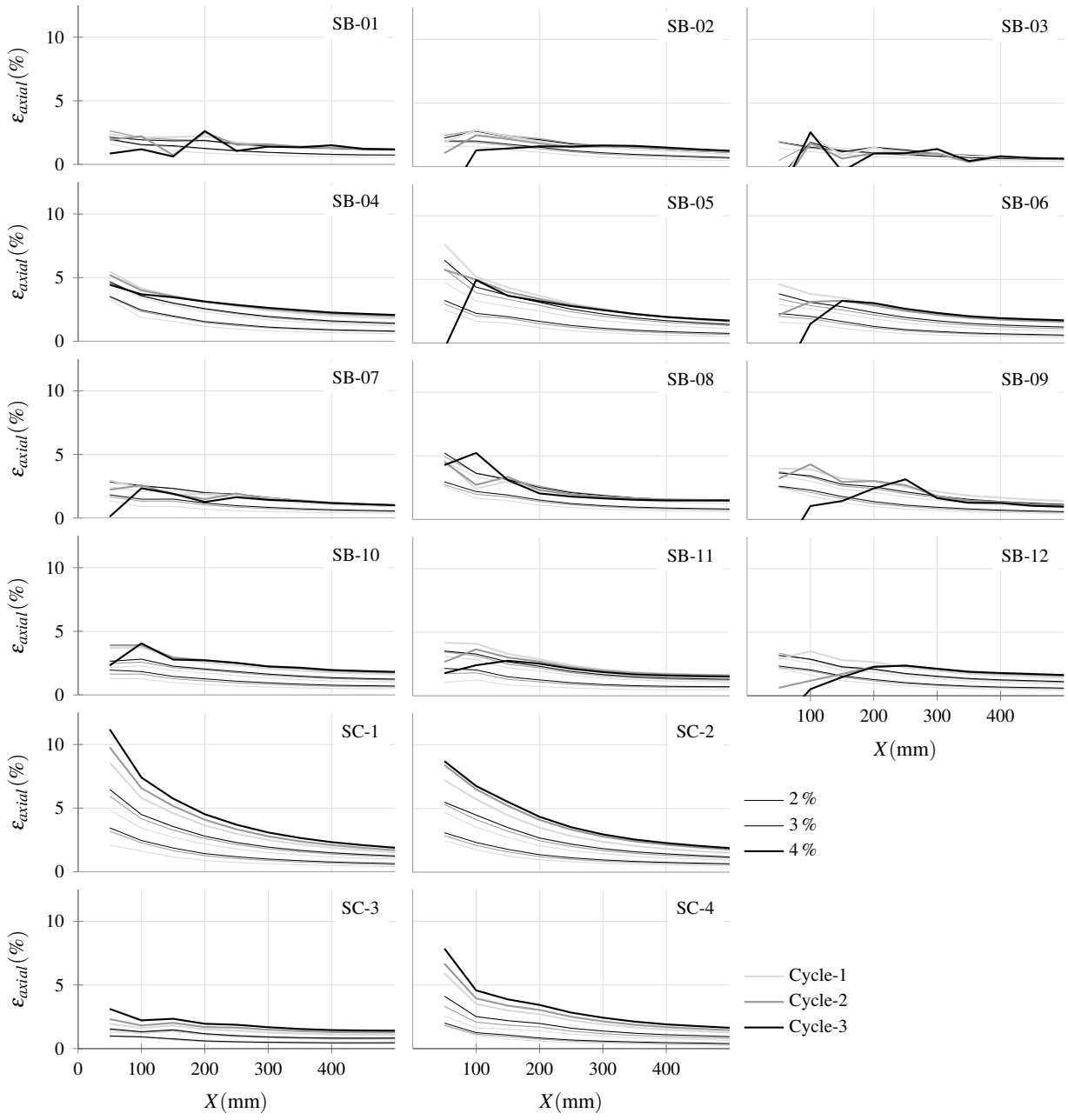

Figure 8: Axial strain profiles for all specimens at the end of 3 (thick lines), 2, and 1 (thin lines) loading cycles at increasing target drifts (2 %, 3 % and 4 %)

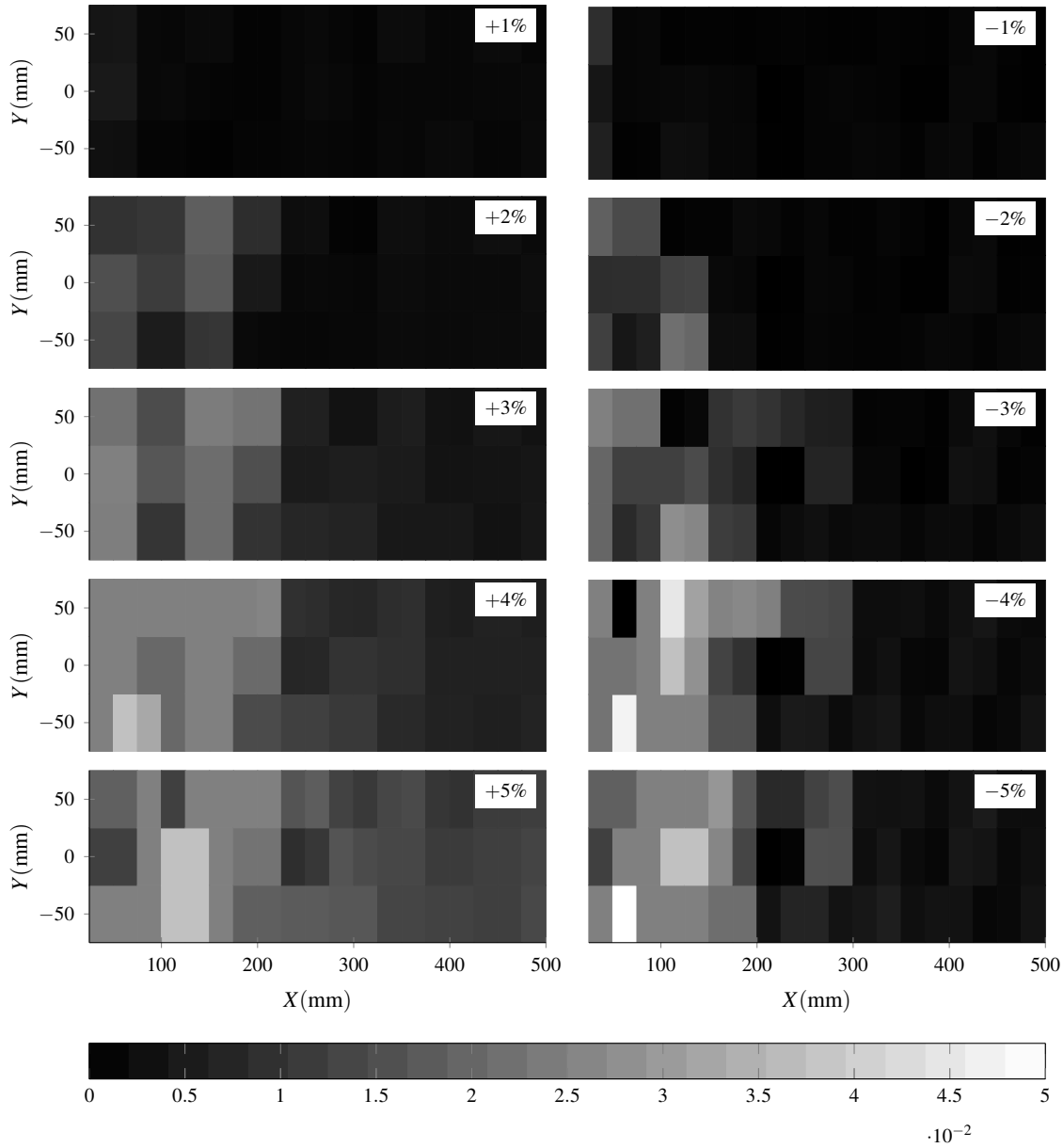

Figure 9: State of shear strain (in %) at peak loading state after three cycles of loading at the indicated target drifts (specimen SB05.) Loading in downwards direction is positive.

influence of repetitive cyclic loading on axial strain development. The strains represented by solid lines after three cyclic repetitions are almost the same as the strains represented by the lighter lines denoting first and second cycles. Observing again the response of specimen SB-04, axial strain is maximum close to the hinge and decreases gradually over the beam span. This distribution can be explained by the development of flexural cracking. Largest flexural cracks appear close to the hinge region and the extent and width of those cracks gradually decreases over the beam span as the does the bending moment. This axial strain distribution implies that the beam response was dominated by flexural behavior. In contrast, the distribution for specimen SB-01 represents a mix of flexural and shear components, especially at larger target drifts. The development of larger axial strains with increasing target drifts in the case of SC series specimens also implies development of stable flexural behavior with any deterioration in resistance.

Typical development of shear strains on concrete surface during progressive loading cycles is illustrated using the reference case of specimen SB-05 in Figure 9 as calucluated using Equation (6). The plots

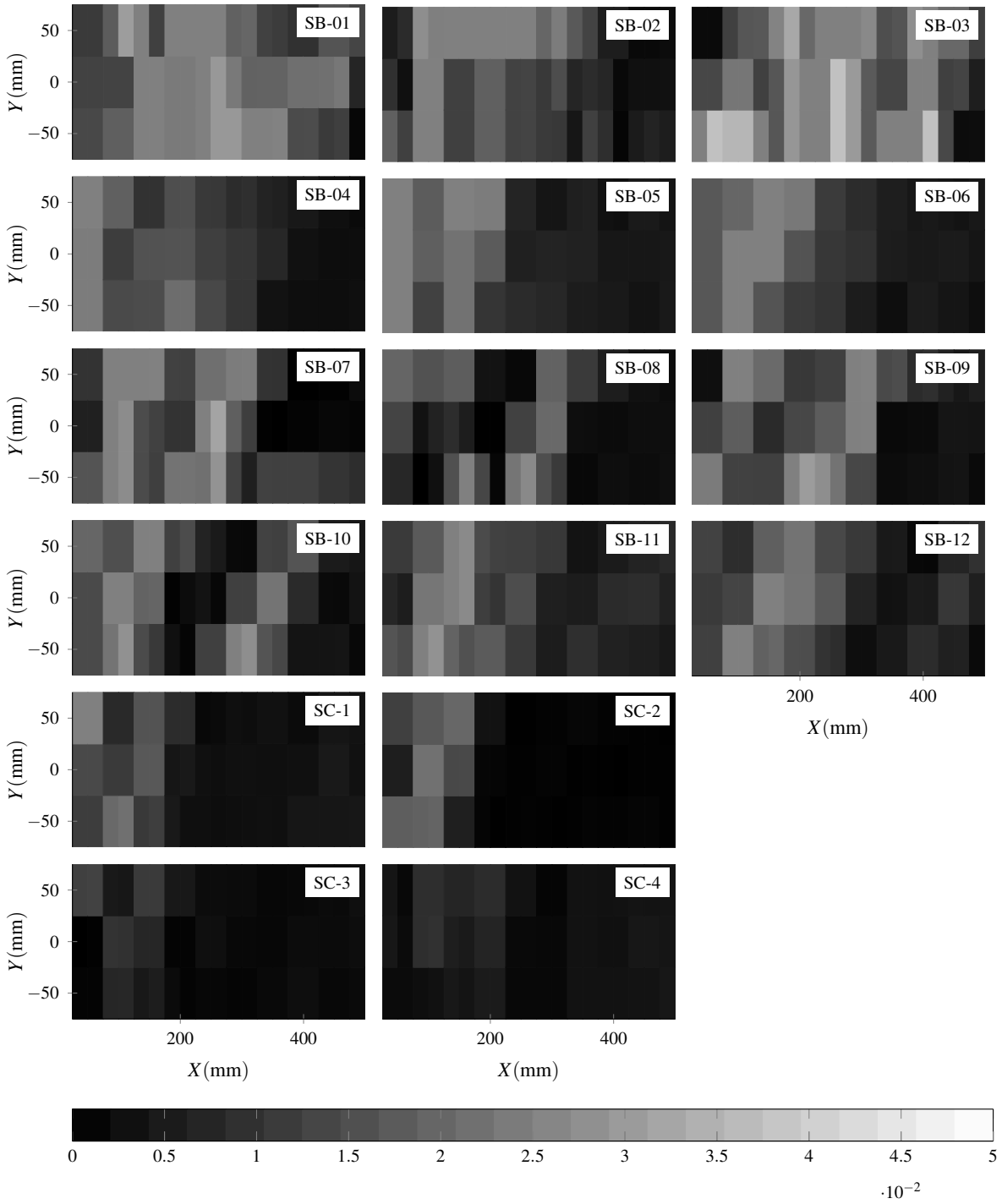

Figure 10: State of shear strain (in %) at peak positive load during second cycle at 4 % target drift.

represent the state of stress at peak load in positive and negative loading directions during the third loading cycle at each indicated target drift level. No regions of any significant shear strain development are observed during the loading cycles at 1 % and 2 % target drift. However, shear strain development starts appearing during 3 % target drift loading cycles and the strain values take a big jump during the 4 % target drift cycles. Loss of resistance was ultimately observed at 5 % target drift cycles [1)] but it can be clearly observed that the state of stress at 5 % target drift does not differ significantly than the one observed at 4 % target drift.

State of shear strain for all specimens at peak positive load during the first cycle at 4 % target drift is expressed in Figure 10 for comparison. Specimens SB-04 to SB-06 with closely spaced stirrups developed comparatively lower strains and only in the hinge region. In comparison, much larger strains and over a larger span were observed in specimens SB-01 to SB-03 at the same loading state. Specimens SB-08 and SB-09 developed relatively lower shear strains but the distribution was spread over the entire span. While strain development was negligible in the SC series specimens.

4. CONCLUSION

An innovative measurement scheme utilizing the principles of photogrammetry was used to record and study cyclic deformation response of RC beams in this report. Photogrammetry enabled observation of surface strains in terms of lateral, axial, and shear at a level of detail not practical using conventional sensors. Effectiveness of closely spaced stirrups in producing a stable flexural response even under comparatively large drift levels was clearly evident from the recorded strain profiles. Final loss of strength was also observed to be related to the development of extensive shear strains in the hinge zone. These findings establish the effectiveness of using photogrammetry to qualitatively study the response of reinforced members in experimental investigations.

ACKNOWLEDGEMENTS

The authors wish to express their gratitude to the Grants-in-Aid for Scientific Research (JSPS KAKENHI) under Grant No. JP16H04446 for the financial support of this research. The first author gratefully acknowledges the support provided by Japanese Government MEXT scholarship program.

REFERENCES

1) Shubham Trivedi. *Experimental investigation of mechanism at ultimate drift capacity in reinforced concrete beams subjected to reversed cyclic loading*. PhD Thesis, University of Tokyo, Tokyo, Japan, 2018.
2) Peng Zhou and Kenneth E. Goodson. Subpixel displacement and deformation gradient measurement using digital image/speckle correlation (DISC). *Optical Engineering*, 40(8):1613–1620, 2001. doi: 10.1117/1.1387992. URL `http://spiedigitallibrary.org/article.aspx?articleid=1098336%20`.
3) Z. Zhang. A flexible new technique for camera calibration. *IEEE Transactions on Pattern Analysis and Machine Intelligence*, 22(11):1330 – 1334, 2000. doi: 10.1109/34.888718.